Observation and modelling of ferromagnetic contact-induced spin relaxation in Hanle spin precession measurements

L. O'Brien, D. Spivak, N. Krueger, T. A. Peterson, M. J. Erickson, B. Bolon, C. C. Geppert, C. Leighton, and P. A. Crowell

Phys. Rev. B **94**, 094431 — Published 26 September 2016
DOI: 10.1103/PhysRevB.94.094431

Observation and modelling of ferromagnetic contact-induced spin relaxation in Hanle spin precession measurements

L. O'Brien[1,2,†], D. Spivak[3], N. Krueger[3], T. A. Peterson[3], M. J. Erickson[3], B. Bolon[4], C. C. Geppert[3], C. Leighton[1], and P. A. Crowell[3]

[1] Department of Chemical Engineering and Materials Science, University of Minnesota, MN, USA.

[2] Thin Film Magnetism, Cavendish Laboratory, University of Cambridge, UK.

[3] School of Physics and Astronomy, University of Minnesota, MN, USA

[4] Department of Physics, Hamline University, MN, USA

Abstract

In the non-local spin valve (NLSV) geometry, four-terminal electrical Hanle effect measurements have the potential to provide a particularly simple determination of the lifetime (τ_s) and diffusion length (λ_N) of spins injected into non-magnetic materials. Recent work, however, has demonstrated that traditional models typically used to fit such data provide an inaccurate measurement of τ_s in ferromagnet/non-magnetic metal (FM/N) devices with low interface resistance, particularly when the separation of the source and detector contacts is small. In the transparent limit, this shortcoming is due to the back-diffusion and subsequent relaxation of spins within the FM contacts, which is not properly accounted for in standard models of the Hanle effect. Here we have used the separation dependence of the spin accumulation signal in NLSVs with multiple FM/N combinations, and interfaces in the diffusive limit, to determine λ_N in traditional spin valve measurements. We then compare these results to Hanle measurements as analyzed using models that either include or exclude spin sinking. We demonstrate that differences between the spin valve and Hanle measurements of λ_N can be quantitatively modelled, provided that both the FM contact-induced isotropic spin-sinking and the full three-dimensional geometry of the devices, which is particularly important at small contact separations, are accounted for. We find, however, that considerable difficulties persist, in particular due to the sensitivity of fitting to the contact interface resistance and the FM contact magnetization rotation, in precisely determining λ_N with the Hanle technique alone, particularly at small contact separations.

[†]Corresponding author: lao24@cam.ac.uk

PACS No's: 72.25.Ba, 72.25.Mk, 85.75-d, 72.25.Rb

By separating charge and spin currents, the non-local spin valve (NLSV) provides a means to probe spin injection and relaxation while minimizing complications from charge current-based effects.[1–3] In the NLSV geometry, the four-terminal electrical Hanle effect, which probes spin precession about an orthogonal magnetic field, in principle provides a simple measurement of the lifetime, τ_S, of spins injected into non-magnetic (*i.e.* para- or diamagnetic) metals (N) or semiconductors (SC). Such measurements have proven accurate in NLSVs with *tunnel barrier* ferromagnet (FM)/N contacts, in which spin relaxation occurs predominantly within the N or SC channel. Indeed, τ_S is typically extracted by fitting the oscillatory perpendicular field-dependence of the Hanle spin accumulation signal ("Hanle curves") using a 1-D solution of the spin-precession-diffusion equation, considering spin relaxation only within the N or SC.[4] Recent studies however, using both graphene and Ag channels,[5–8] have shown that with *low spin resistance (i.e. diffusive)* contacts this approach breaks down, with deviations being particularly noticeable when the FM contact separation (*d*) is small relative to the spin diffusion length, $\lambda_N = \sqrt{\tau_S D}$, where D is the electron diffusivity. In this regime, Hanle curves at different *d* can no longer be fit using a single τ_S. Instead, the fits yield lifetimes that not only appear to be *d*-dependent, but are also substantially smaller than the true τ_S.

A general consensus has emerged that in metals this discrepancy is predominantly due to a spin sinking effect, *i.e.,* additional spin relaxation when injected spins diffuse back into the FM contacts.[5–7,9,10] In materials such as graphene the situation is more complex. Although spin sinking dominates in diffusive contacts, at finite interface resistance additional mechanisms, such as relaxation from adsorbates[11] and other contact-induced relaxation sources[12], have been found to mask the intrinsic spin lifetime. For all cases, the effect of spin sinking is negligible when high spin resistance tunnel contacts are employed but becomes significant in the diffusive contact regime. A number of works have attempted to model this FM contact-induced spin sinking,[3,6,9,10] the extent of which is determined by the ratio of the spin resistances of the channel, R_N (or R_{SC}), to that of the FM injector/detector, $R_{FM}^{inj/det} = R_{FM} + R_I$. Here, the channel spin resistance $R_N = \rho_N \lambda_N / w_N t_N$ with ρ_N, w_N, t_N the channel resistivity, width, and thickness; $R_{FM} = \rho_{FM} \lambda_{FM} / w_{FM} w_N$ represents the intrinsic FM spin resistance with $\rho_{FM}, w_{FM}, \lambda_{FM}$ the FM resistivity, contact width, and spin diffusion length; and R_I is the contact interface resistance. Each model differs in its specific treatment of spin sinking, considering either longitudinal[3] (neglecting sinking of the spin component orthogonal to the FM magnetization), isotropic[9,13] or anisotropic[6] sinking. Overall, such models successfully capture the enhancement of the effective spin relaxation rate as d decreases; however, each predicts considerably different behavior at small d. Quantitatively assessing the role of any of these proposed mechanisms using Hanle measurements alone has been difficult. Clearly, in the diffusive limit the shape of the Hanle curve is no longer solely determined by τ_s, and becomes sensitive to a number of additional parameters, including R_N, R_{FM} and R_I. The impact of the different sinking mechanisms, and therefore the accuracy of each model, remains unclear. In addition to this uncertainty, effects such as finite device size and the rotation of the FM contact magnetization under an applied field also play a critical role in determining the overall Hanle curve shape.

In this paper we demonstrate that the Hanle effect in four-terminal diffusive contact NLSVs can be successfully modeled if isotropic spin-sinking is included. Our simulations also show how the full 3D character of these devices, particularly the finite thickness of the spin channel, must be accounted for in the limit $d < \lambda_N$. By first fitting the d-dependent decay of the NLSV spin accumulation signal, explicitly accounting for spin sinking,[14] we obtain an unambiguous value of λ_N, with which we compare the diffusion length extracted from Hanle measurements. To quantify any discrepancy between NLSV and Hanle measurements, we explicitly define this Hanle diffusion length as an effective one, λ_{eff} (with $\lambda_{eff} = \sqrt{\tau_{eff} D}$). Throughout this paper, λ_{eff} will refer to the spin diffusion length as determined by fitting Hanle data (either experimental or simulated) to a particular model. We consider several such models, starting with the traditional Hanle analysis in which spin sinking is neglected completely. Because the effects of spin sinking are not properly accounted for in the traditional Hanle analysis, λ_{eff} in this case will always be smaller than λ_N, with the suppression most marked at the smallest separations. We find that modelling including only isotropic contact-induced spin sinking accounts for this phenomenon, with no need to invoke additional relaxation mechanisms such as anisotropic spin sinking[6] or surface relaxation.[15–18] By comparing experiments and 3D simulations to various 1-D models over a significant range of parameter space, we have also assessed the difficulties in determining λ_N using Hanle measurements alone. In particular, the considerable sensitivity of the Hanle curve shape to R_I, as well as to rotation of the FM contact magnetization, make the determination of λ_N highly imprecise at small d/λ_N. Although spin sinking is important at all contact separations, we find that deviations at small d (less than the spin diffusion length) can only be accounted for by using a 3D model that incorporates the full device geometry. The increased accuracy of these 3D simulations relative to 1D is traced back to the non-zero channel thickness and finite contact size, which must be accounted for in order to avoid overestimation of the diffusive spin current flowing into the FM source or detector as $d \to 0$. This consideration will become increasingly important as lateral device dimensions shrink further, and future experiments begin to probe this regime.

We first present results from experimental measurements of the non-local spin accumulation signal as a function of both contact separation d and applied field H. The inset to Fig. 1b shows the experimental geometry and contact configuration employed. The FM contacts are shown in red and the N channel in gray. Devices with Fe, $Ni_{80}Fe_{20}$ and Co FM electrodes (99.95 % purity) and Al and Cu channels (99.999 % purity) were investigated. We note that these source purities do not necessarily reflect the ultimate composition, due to potential contamination during deposition[16] and to FM/N interdiffusion.[19] The devices were fabricated using electron beam lithography and a suspended resist mask. Multi-angle electron-beam evaporation under ultra-high vacuum (base pressure 10^{-10} Torr) was used to deposit the FM and N sequentially without breaking vacuum. Nominally, $t_N = 200$ nm, $w_N = 150$ nm, $t_{FM} = 16$ nm, $w_{FM}^{inj} = 160$ nm (injector) and $w_{FM}^{det} = 110$ nm (detector), and the measured 5 K resistivity (ρ) values were: $\rho_{Al} = 2.5$ μΩcm, $\rho_{Cu} = 0.8$ μΩcm, $\rho_{Fe} = 13$ μΩcm, $\rho_{NiFe} = 30$ μΩcm and $\rho_{Co} = 19$ μΩcm. For all devices, $R_{FM}/R_N \leq O(0.1)$ at all T. Probing R_I directly through 3-terminal measurements, we establish $R_I < R_N$ for our devices, meaning that they operate in the diffusive limit. We note, however, as is typically the case for all-metallic devices,[20] that only an upper limit of $R_I \leq O(R_{FM})$ may be placed on contact transparency due to finite current spreading (see the Supplementary Information of Ref. [19]).

In the non-local geometry, a spin-polarized bias current, I, injected from one FM generates a diffusive pure spin current in the N channel between the two FMs. The trans-impedance ($R_{NL} = V_{NL}/I$) then provides a direct measure of the spin accumulation at the FM detector a distance *d* along the channel, dependent on the relative FM orientation. Figs. 1a and b show the evolution of R_{NL} under in-plane ($H_{\parallel}$) and out-of-plane (OOP; $H_{\perp}$) magnetic fields, for an Fe/Al NLSV with $d = 1$ μm at $T = 5$ K. As is typical, an *H*-independent background has been removed, in this case -632 μΩ.[21,22] As shown in Fig. 1a, using $H_{\parallel}$ to switch between parallel (P) and anti-parallel (AP) configurations of the two FMs provides the non-local spin accumulation signal, $\Delta R_{NL} = R_P - R_{AP}$. The gray arrows illustrate the evolution of R_{NL} with $H_{\parallel}$, starting from negative saturation. By reversing the direction of $H_{\parallel}$ once the AP state is reached, we measure R_{AP} at zero field, avoiding changes in the signal due to rotation of the FMs in finite $H_{\parallel}$. For $H_{\perp}$ (Fig. 1b) a damped oscillation is observed for $R_P(H_{\perp})$ and $R_{AP}(H_{\perp})$, due to spin precession, which is convolved with the finite τ_s and a temporal distribution associated with spin diffusion (the Hanle effect[1,4]). As $H_{\perp}$ increases, the in-plane spin accumulation is supressed, and $R_P(H_{\perp})$ approaches $R_{AP}(H_{\perp})$. At fixed separation, the widths of these Hanle curves increase with decreasing τ_s. In metals,

τ_s is typically short (of order 10 ps) and so the curves are wide (often > 10 kOe). By fitting such curves, τ_{eff} (and therefore λ_{eff}) may be extracted, which is non-trivially related to τ_s, as discussed above.

At large fields, $H_\perp$ causes the magnetization of the FMs to rotate OOP, reducing the in-plane component. Eventually, when $H_\perp \geq H_K$ (the OOP anisotropy field), both FMs are oriented OOP, there is no precession, and $R_{NL}(H_\perp) = R_P(H_\perp) = R_{AP}(H_\perp)$, regardless of the initial contact preparation, as seen in Fig. 1b. Using $\Delta R_{NL}(H_\perp) = R_P(H_\perp) - R_{AP}(H_\perp)$, as opposed to $R_P(H_\perp)$ or $R_{AP}(H_\perp)$ alone, removes the contribution from the OOP spin accumulation generated by the perpendicular component of the contact magnetization. We note, however, that this procedure does not account for the reduction in the in-plane spin accumulation as a result of the magnetization rotation. It is therefore preferable to choose a system in which the effects of magnetization rotation are as small as possible. Considering all of these factors, Fe/Al is an ideal FM/N combination for Hanle measurements, particularly at small d. The relatively long τ_s in Al (~40 ps at 5 K for our devices) means that the Hanle curve is relatively narrow (of order 1 kG), while the large saturation magnetization (and therefore H_K) of Fe ensures a sufficiently wide field range over which R_{NL} can be probed before the contact rotation becomes significant.

To assess the suppression of λ_{eff} by spin sinking in the contacts quantitatively, we first use NLSV measurements of $\Delta R_{NL}(d)$, carried out with an in-plane field, to extract $\lambda_N(T)$. As d increases, ΔR_{NL} decays approximately exponentially on the length scale λ_N, as shown for Fe/Al devices at various T in Fig. 2a. The deviation from simple exponential behavior at small d is expected, due to the aforementioned spin sinking at the FM contacts. This is described by an analytical solution based on the Valet-Fert formulation of the 1-D spin diffusion model:[23]

$$\Delta R_{NL} = 4\frac{\alpha^2}{(1-\alpha^2)^2}\frac{R_{FM}^{inj}\, R_{FM}^{det}}{R_N}\frac{\exp\left(-\dfrac{d}{\lambda_N}\right)}{\left[1+\dfrac{2R_{FM}^{inj}}{(1-\alpha^2)R_N}\right]\left[1+\dfrac{2R_{FM}^{det}}{(1-\alpha^2)R_N}\right]-\exp\left(-\dfrac{2d}{\lambda_N}\right)} \qquad (1),$$

where α is the FM current polarization. Here R_{FM}^{inj} and R_{FM}^{det} are different because of the different sizes of the two contacts. Because Eq. 1 explicitly accounts for longitudinal spin sinking, fitting $\Delta R_{NL}(d)$ provides a direct means to measure λ_N. Note that here $\alpha(T)$, $\lambda_{FM}(T)$ and $\lambda_N(T)$ are unknowns, while $\rho_N(T)$ is determined from four-point measurements on the tested NLSVs, and $\rho_{FM}(T)$ is measured on nominally identical FM nanowires. As discussed previously,[19] the existence of three unknowns means that either $\alpha(T)$ or $\lambda_{FM}(T)$ should be constrained. However, because λ_N is determined predominantly by the d dependence of ΔR_{NL} alone, the extracted value is insensitive to the particular constraints chosen for α and λ_{FM}.[19] Shown as solid lines in Fig. 2(a) are fits for the particular case where λ_{FM} is fixed at 4 nm[19] (using the phenomenological relationship between ρ_{FM} and λ_{FM} as observed in ref. [24]), resulting in the $\lambda_N(T)$ shown in Fig. 2c (open squares). Significantly, $\lambda_N(T)$ is monotonic, saturating at ~ 700 nm at low *T*. This monotonic temperature dependence is characteristic of Al channels. Dilute local moments from interdiffused 3*d* transition metals are not supported in Al, and thus the recently demonstrated Kondo-related suppression of spin accumulation at low T does not occur (see Ref. [25]). In contrast to λ_N, the value of α determined from fitting depends sensitively on the particular constrained values of R_{FM} and λ_{FM}, as well as any interfacial resistance R_I that is present. Due to this interdependence it is not possible to uniquely ascertain a value for all three parameters (R_{FM}, λ_{FM}, and R_I) from NLSV measurements alone. We note, however, that consistency between the Hanle and NLSV measurements (see Figures 2 and 3) can be found for $\alpha(T = 5\ K) \sim 0.3$, $\lambda_{FM} = 4$ nm, and $R_I = 7R_{FM}$. We will return to the relative values of R_I and R_{FM} below.

With $\lambda_N(T)$ established from the spin valve measurements, we now compare it to $\lambda_{eff}(T, d)$ as determined from $\Delta R_{NL}(H_\perp)$. Since λ_N is obtained directly from $\Delta R_{NL}(d)$, this represents an unambiguous quantity with which to compare λ_{eff}. We emphasize again that this λ_{eff} is an effective diffusion length obtained from fitting Hanle curves with the typical integral expression,[26] in which the spin current flowing into the FM contacts is ignored (this assumption would be appropriate for tunnel barrier contacts). In this limit:

$$\Delta R_{\mathrm{NL}}(H_\perp) = \mathrm{S}_0 \int_{-w_{\mathrm{FM}}^{\mathrm{inj}}}^{0} \int_{d}^{d+w_{\mathrm{FM}}^{\mathrm{det}}} \int_0^\infty \frac{1}{\sqrt{4\pi D t}} \exp - \frac{\left(x_{\mathrm{inj}} - x_{\mathrm{det}}\right)^2}{4Dt} \cos(\omega_{\mathrm{L}} t) \exp\left(-\frac{t}{\tau_{\mathrm{eff}}}\right) dt\, dx_{\mathrm{det}}\, dx_{\mathrm{inj}} \quad (2),$$

where ω_L is the Larmor frequency ($\omega_L = \gamma B$, with γ the gyromagnetic ratio and *B* the magnetic flux density), and S_0 is a normalization factor determined by the zero-field signal. The experimental data in Fig. 2b (colored points) show $\Delta R_{NL}(H_\perp)$ for various d at $T = 5$ K, for the same Fe/Al NLSVs shown in Fig. 2a. The data are normalized to the $H_\perp = 0$ values for ease of comparison. Also, although data were taken for both positive and negative $H_\perp$ (Fig. 1b), only the symmetric component, $\Delta R_{NL,sym} = [\Delta R_{NL}(H_\perp) + \Delta R_{NL}(-H_\perp)]/2$, is shown. The experimental curves are observed to narrow with increasing d. This occurs because as d increases the mean spin transit time from injector to detector increases, creating a larger average precessional angle, and thus greater modulation of ΔR_{NL} for a given $H_\perp$. For fitting, the reduction of the in-plane spin component due to rotation of the FM contacts OOP is taken into account by multiplying the integrand in Eq. 2 by $(1 - (H_\perp/H_K)^2)$, which assumes coherent rotation in the presence of a purely uniaxial anisotropy. Here, H_K is the shape anisotropy field of the contacts, which is calculated numerically using the saturation magnetization $\mu_0 M_s = 2.1$ T and the FM nanowire dimensions.[27] Only τ_{eff} and S_0 are free parameters in the fits; $D(T)$ is determined from the measured $\rho_N(T)$ using the Einstein relation, $\rho_N(T)^{-1} = N(E_F)D(T)e^2$, with $N(E_F)$ the density of states at the Fermi level and e the electronic charge. For large separations, *d,* for which well-defined lobes of opposite sign appear in the Hanle curves, this value of *D* is essentially the same as that which would be obtained by making it a fitting parameter. At small separations, however, it is not possible to determine *D* and τ_s independently from the Hanle curves alone. In the case of conventional metals, where screening is effective, there is no *a priori* reason to expect the spin and charge diffusion constants to differ, and so constraining *D* using the Einstein relation is preferable to making it a free parameter in Hanle fits.[28] Because $D(T)$ is constrained by experiment, variations in $\lambda_{eff}(T)$ directly reflect changes to the best-fit value of τ_{eff} alone. Because Eq. 2 does not account for spin sinking, we anticipate $\lambda_{eff} < \lambda_N$ at all d, with the effect being most pronounced as $d \to 0$. Fig. 2c shows the fit results for $\lambda_{eff}(T) = \sqrt{\tau_{eff} D}$ for various d, directly comparing to λ_N (fitted curves at $T =$ 5 K are shown in Appendix A). The substantial underestimation of λ_N as d decreases (particularly below 1500 nm) confirms the qualitative expectation. To further emphasize the above, Fig. 2b also shows the *predicted* Hanle curves from Eq. 2 (solid lines), *assuming* $\lambda_{eff} = \lambda_N$ (*i.e.* $\tau_{eff} = \tau_S$). Below $d = 1500$ nm ($\sim 2\lambda_N$) the experimental data and the predictions without accounting for spin sinking differ greatly[29].

To facilitate quantitative comparisons, Fig. 3b shows λ_{eff}/λ_N *vs*. the reduced separation, d/λ_N. Each dataset shown with closed symbols represents a tested NLSV device with the indicated d value, while the open symbols and lines are modelling/simulation results that will be discussed below. Experimental data are shown for two sets of devices (closed blue or red symbols). As T increases, λ_N decreases (Fig. 2c), and thus, by varying T, we obtain a range of d/λ_N for each measured device. From Fig. 3b a clear trend emerges, with a near monotonic drop in λ_{eff}/λ_N as d/λ_N decreases. Note that the gray band shown around $\lambda_{eff}/\lambda_N = 1$ indicates the size of the systematic errors in λ_N and D arising from the NLSV fitting described above. This error follows primarily from uncertainty in the measured device parameters, *e.g.*, ρ_N, t_N and d, combined with the limitations in the precision of fits over only 3 decades in ΔR_{NL} (limited by the practicalities of measuring sub-nV signal sizes at large separations). This systematic error is the dominant uncertainty when comparing λ_{eff}/λ_N values. (Errors bars from fitting λ_{eff} are in fact small, approximately the data point size.) As all data from a device set (blue or red symbols) use the same values of $\lambda_N(T)$ and $D(T)$, any error in either quantity will cause a systematic shift of the entire set. The apparent lateral shift in the data of Fig 2c for different device batches, as well as the fact that λ_{eff} apparently exceeds λ_N in some cases, are consistent with the magnitude of this systematic error.

Having presented experimental results on the underestimation of λ_N due to spin sinking, we now turn to modelling these observations. Several approaches have investigated the effect of spin sinking on Hanle curves, in particular considering precession-diffusion in 1-D.[3,6,9–13] We do so here by solving the steady-state spin drift-diffusion equation with precession,[30] considering the full device geometry:

$$\frac{\partial \vec{p}}{\partial t} = D\nabla^2 \vec{p} - \frac{\vec{p}}{\tau_s} + \vec{\omega}_L \times \vec{p} + \vec{G}(\vec{r}) = 0, \tag{3}$$

where the spin polarization $\vec{p}$ is defined on a three-dimensional grid of cells, each 55 x 25 x 25 nm^3, with total dimensions 7.7 μm long, $w_N = 150$ nm wide, and $t_N = 200$ nm thick. This is shown schematically in Fig. 3a. The Larmor frequency vector $\vec{\omega}_L$ is parallel to the applied field, and the source term $\vec{G}(\vec{r})$ is set to a non-zero constant only in the cells just above the ferromagnetic injector. Neumann boundary conditions are applied, so that no spin current flows through the boundaries of the system. We assume that the spin current flowing into the FMs from the N channel is determined by the parallel spin resistances of N and FM, and that the spin current flowing into the FMs is equivalent to an additional source of spin relaxation in the boundary cells at the FM/N interface (see Fig. 3a). This mapping allows the Neumann boundary condition to be maintained without including the FM explicitly. We note that such boundary conditions are equivalent to assuming isotropic spin sinking in a 1-D model. In other words, the spin sinking current is presumed to be independent of the *orientation* of the spins in the boundary cells. In steady state, the total relaxation rate in a cell must be equal to the total spin current flowing into that cell, and so this treatment of spin sinking is equivalent to defining a total relaxation rate:

$$f_s^* = \frac{1}{\tau_s}\left[1 + \frac{\rho_N \lambda_N}{\rho_{FM}\lambda_{FM}}\left(\frac{\lambda_N}{\Delta z}\right)\right] \approx \frac{\rho_N {\lambda_N}^2}{\rho_{FM}\lambda_{FM}\Delta z}\frac{1}{\tau_s}, \tag{4}$$

in the cells above the detector ferromagnet, where Δz is the cell thickness. A derivation of Eq. (4) is provided in Appendix B. Hence the spin relaxation time in these boundary cells is ${f_s^*}^{-1}$, while it is simply τ_s everywhere else. At $T = 5$ K, $\tau_{s,Al} = 42$ ps, giving $f_s^* = 24$ ps^{-1}, and so the cells above the FM are nearly ideal spin sinks. The spin drift-diffusion equation is evolved forward in time until a steady-state is reached, and the detected spin accumulation is determined by averaging the projection of the spin polarization over the detector boundary cells. This process is repeated at each $H_\perp$ to generate a Hanle curve. The effect of FM rotation is accounted for in an identical manner as in the fits using Eq. 2, *i.e.*, the in-plane polarization is reduced by coherent rotation under the combined effects of the applied field $H_\perp$ and the anisotropy field H_K.

By modelling $\Delta R_{NL}(H_\perp)$ in the above manner, we construct a series of numerical Hanle curves which may then be fitted using Eq. 2 to extract λ_{eff}/λ_N for each separation. We emphasize that this method explicitly accounts for finite contact size and channel thickness, as well as the fact that any spins that diffuse into the open channel are not absorbed by the FM contacts. This is distinct from 1D treatments, where spins reaching the end of the channel are entirely sunk by the FMs. Our approach, however, considers no additional spin relaxation mechanisms *e.g.*, anisotropic transverse spin relaxation[6] (the dependence of the spin sinking current on the orientation of the spin polarization in the boundary cells) or relaxation at either the N/vacuum or N/substrate interfaces.[15–17] The open black squares in Fig. 3b show the results obtained using this method, with the dashed line providing a guide to the eye. Comparing with the experimental data, one sees a systematic overestimation of the spin sinking effect from modelling. We account for this phenomenologically by including a finite interface resistance-area product, $R_I A_I$, which is added in series to $\rho_{FM}\lambda_{FM}$ in Eq. 4 in an identical manner to its consideration in the 1-D models, *i.e.* $\rho_{FM}\lambda_{FM} \rightarrow\ R_I A_I + \rho_{FM}\lambda_{FM}$. In assessing the overall agreement between the model and experiment, we consider the previously mentioned systematic error in λ_{eff}/λ_N, as represented by the gray band in Fig 3(b,c). This band arises as all data in the figure rely on the same values of λ_N and D; any error in their estimation will thus produce a systematic shift for *all* experimental points. As both quantities are experimentally determined, they suffer from any limitations in the accuracy of a number of parameters. One feasible mechanism by which a shift could occur is from estimating D. As it is determined using ρ_N, any overestimation of channel cross-sectional area (e.g., due to a non-square wire cross-section) consequently causes a systematic underestimation of D. To a good approximation, this systematic error will cause an underestimation of τ_s in fitting across all devices, meaning that the data will be shifted along the y-axis. By varying $R_I A_I$, and considering such a potential shift, we find closer agreement between experiment and modelling for $R_I \sim 7\ R_{FM}$ ($R_{FM}^{inj/det} = 8\ R_{FM}$), shown as the open black circles in Fig. 3b. In particular, this value of R_I reproduces the approximately 50% suppression of λ_{eff}/λ_N at small d that is observed experimentally. Note that such an increase in R_I would be difficult to detect in direct '3-terminal' measurements of the contact resistance. Furthermore, a contact resistance in this range maintains the condition $R_N > R_I, R_{FM}$. Consistency between the NLSV and Hanle approaches can be found with $R_I = 7\ R_{FM}$, $\alpha\ \approx\ 0.3$, and $\lambda_{FM} = 4$ nm, values that are comparable to literature results[24,31,32]. As a further comment regarding R_I, it should be noted that values of $R_I \sim R_{FM}$ are invariably found for metal-metal interfaces, with $R_I A_I$ in the range of $\sim$1 fΩm^2 readily observed for many FM/N. Indeed the observed value of 3.5 fΩm^2 here is in very good agreement with values found in other Fe/Al spin valves[33], where $RA_{Fe/Al}$ was observed to be 4.1 ± 0.3 fΩm^2. In general, a non-zero $R_I A_I$ should not, in itself, be considered a signature of a 'non-ideal' device, but rather a property of the interface itself.

As further evidence for the origin of the underestimation of τ_s in Hanle analyses which ignore spin sinking, in Fig. 3c we plot λ_{eff}/λ_N vs d for multiple FM/N combinations. By virtue of the fact that the spin resistances R_{FM} are much smaller than R_N for each combination, the data all follow a similar trend. This confirms expectations, as well as the general origin of the underestimation: Spin diffusion into FMs is greatest in NLSV devices with substantial spin resistance mismatch between the contacts and the N channel. Clearly, the spin resistance mismatch in the devices shown here is small compared to that of *e.g.*, FM/graphene NLSVs,[5,7,8] and hence the effect is less pronounced. Despite this, the suppression is measurable in the metallic case, and follows the expected trend for all materials combinations tested.

Although our 3-D simulations account for the observed trends in λ_{eff}, it is nevertheless instructive to compare with previous models that account for spin sinking. Doing so highlights the difficulties inherent in extracting τ_s from Hanle measurements alone in the all-metallic, diffusive contact regime. We consider three particular cases: Spin transport in the presence of longitudinal[3] (no transverse), isotropic[9,13] or anisotropic sinking.[6] In principle, using such models to fit either the experimental data or 3-D numerical simulations, with appropriately constrained R_I/R_N, should result in $\lambda_{eff} = \lambda_N$ for all d.

We consider first the case where only the longitudinal component of the spin accumulation (*i.e.,* the component parallel to the contact magnetization) is considered to be sunk by the FM, as assumed in Ref. 3. In this model, the transverse spin accumulation within the N remains unaffected by the presence of low spin resistance contacts. Ignoring sinking of the transverse spin accumulation and using a 1-D model with only longitudinal sinking, which we refer to as the longitudinal model, the Hanle curve width, and in-particular the zero-crossing point of the curve (when the spin accumulation has, on average, precessed through an angle $\pi/2$), is found to be independent of the degree of spin sinking. Fig. 4a illustrates this fact, showing normalized Hanle curves generated from such a model ($d = 2$ µm, $\lambda_N =$ 733 nm, $D =$ 14.8 µm^2/ns; parameters appropriate for our devices at 5 K), demonstrating this independence. For comparison, the modelled isotropic sinking curve for identical conditions ($R_N/R_{FM}^{Inj/Det} = 32$) is also shown in Fig. 4a using filled circles. As was identified in Refs [6,29], and observed here in both experiment and simulation, substantial widening of the Hanle curve occurs in the limit of diffusive interfaces. As such, it is impossible to fit the observed curves using this longitudinal model, because the field at which the zero crossing occurs in the model is fixed, in complete disagreement with the experimental data of Fig. 2b. If this is ignored, however, Fig. 4b shows parameters extracted from an attempt to fit the simulated data considering only longitudinal sinking. The data are shown for various values of $R_{FM}^{inj/det}$, constrained to the same value in both the simulation and longitudinal spin sinking model. When spin sinking is appreciable, *i.e.*, when $R_N/R_{FM}^{inj/det} > 1$, this method results in a systematic underestimation of λ_N at intermediate separations, and so λ_{eff} is found to decrease with decreasing d/λ_N. At small d/λ_N, however, the average spin transit time is short enough that little field-induced precession occurs, and the Hanle curve no longer crosses zero. In this limit, little transverse spin accumulation exists for all $H_\perp$, and so the Hanle curves are largely insensitive to transverse sinking. Consequently, at small d/λ_N the longitudinal model (which neglects transverse spin sinking) more accurately reflects experiment than at large separations, where the transverse spin accumulation becomes significant. For this reason, a characteristic (but completely artificial) minimum develops in $\lambda_{eff}(d)$, which increases towards λ_N as $d/\lambda_N \to 0$.

We next consider the case of isotropic spin sinking. To establish an expression for $\Delta R_{NL}(H_\perp)$ we follow the treatment of refs [9,13], obtaining an analytical form for 1-D spin diffusion in the limit of transparent interfaces:

$$\Delta R_{NL}(H_\perp) = \mathrm{Re}\left[\frac{4\alpha^2}{(1-\alpha^2)^2}\frac{R_{FM}^{inj}\,R_{FM}^{det}}{R_\omega}\,\frac{\exp\left(-\dfrac{d}{\lambda_\omega}\right)}{\left(1+\dfrac{2}{1-\alpha^2}\dfrac{R_{FM}^{inj}}{R_\omega}\right)\left(1+\dfrac{2}{1-\alpha^2}\dfrac{R_{FM}^{det}}{R_\omega}\right)-\exp\left(-\dfrac{2d}{\lambda_\omega}\right)}\right], \qquad (5)$$

with $\lambda_\omega = \lambda_N/\sqrt{1+\mathrm{i}\,\omega_L\tau_s}$ and $R_\omega = \rho_N\lambda_\omega/w_N t_N$. The spin resistances R_{FM}^{inj} and R_{FM}^{det} of the FM injector and detector include the interface resistance R_I in the same manner adopted for Eq. 1. We note that when $H_\perp = 0$, Eq. 5 is in fact identical to Eq. 1. For comparison with both 3-D modelling and experimental data, the black stars and open triangles in Fig. 3b indicate the extracted λ_{eff}/λ_N from fitting curves generated by Eq. 5 [for the cases $R_{FM}^{Inj/Det} = R_{FM}$ (stars) and $R_{FM}^{Inj/Det} = 8R_{FM}$ (open triangles)] to a tunnel barrier model (*i.e.*, Eq. 2). As would be anticipated, given that both account for spin sinking in a similar manner, there is very close agreement between the 3-D simulation and the 1-D model for most d values. A slight systematic offset is observed in the $R_I = 0$ data, which is likely associated with the approximations made in establishing Eq. 4. There is, however, a notable departure between 3D and 1D for $d/\lambda_N < 1$. In particular, the d-dependence proposed in Ref. [9] implies that $\lambda_{eff} \rightarrow \lambda_N R_I / R_N$ (<0.1 λ_N) in the zero d limit, which is clearly not the case in 3-D (see Fig. 3b). The increase in λ_{eff} at low d between the 1D and 3D models can be attributed to the finite values of t_N and w_{FM}. In devices where t_N is an appreciable fraction of λ_N, there is a sufficiently large volume of N above the contacts to "source" the spin current that is drawn at the interface. Even as $d \rightarrow 0$, the average relaxation rate in the channel is not overwhelmed by the spin sinking effect, and the degree of spin sinking is therefore significantly smaller than in the 1-D case. From this observation we see that when λ_N is comparable to t_N, 1-D models may drastically overestimate the spin sinking effect at small d . In the limit $d/\lambda \gg 1$, the thickness of the channel is irrelevant, and the suppression of λ_{eff} relative to λ_N is determined entirely by the ratio of the spin current drawn by the FM relative to the integral of the spin relaxation rate between the contacts. Only at small d does the channel thickness become relevant. Experimentally, as we remain in the regime where $d \sim \lambda_N$, this departure from the ideal 1-D case is not observed. However, we predict that as the contact separation in metallic devices is decreased below those achieved in this study and other previous work, the full 3-D character of the channel will need to be considered. We note that in NLSVs based on 2-D materials (*e.g.*, graphene) the condition $t_N \ll \lambda_N$ makes the 1-D approach of Ref. [9] appropriate at all separations.

To emphasize the overall challenge in accurately modelling experimental Hanle curves in the diffusive limit, we next demonstrate the sensitivity of λ_{eff} to errors in the FM spin resistance. To illustrate this point, which applies regardless of the particular model used, we first generate a series of Hanle curves, at various d, using Eq. 5. These model data are generated for the case of $\lambda_N = 733$ nm, $\rho_{FM}\lambda_{FM} = 0.52$ fΩm^2, $D = 14.8$ μm^2 (appropriate for our devices at *T* = 5 K) with $R_I = 0$, *i.e.,* in the ideal transparent limit. These results correspond to an ideal case in which λ_N, R_I and $\rho_{FM}\lambda_{FM}$ are known exactly. We then attempt to re-fit the model data, again using Eq. 5, in a manner similar to that which would be applied when fitting the results of an actual experiment in which R_I and/or $\rho_{FM}\lambda_{FM}$ are *not* known precisely. We assume some experimental estimate of the degree of spin sinking has been made, either through calculation or direct measurement of $\rho_{FM}\lambda_{FM}$ and $R_I A_I$. Because both are combined in series to give the total FM spin resistance, used to set R_{FM}^{inj} and R_{FM}^{det} in Eq. 5, it is sufficient for a single *RA* product, $R_{est}A_{est}$, to be defined for this estimate: $R_{est}A_{est} = \rho_{FM}\lambda_{FM} + R_I A_I$. The deviation between $R_{est}A_{est}$ and $\rho_{FM}\lambda_{FM}$ is the systematic error in the estimate of FM spin sinking. Fixing $R_{est}A_{est}$ leaves only τ_{eff} as a free parameter. In this case, λ_{eff} represents the best-fit value of the diffusion length in the N from fitting the model data to Eq. 5. Fig. 5a displays the extracted λ_{eff}/λ_N for various values of $R_{est}A_{est}/\rho_{FM}\lambda_{FM}$. As expected, when $R_{est}A_{est} = \rho_{FM}\lambda_{FM}$ (green triangles), the fit reproduces the model data exactly and λ_N is faithfully extracted ($\lambda_{eff}/\lambda_N = 1$). The most important feature of Fig. 5a, however, is the dramatic change in λ_{eff} when $R_{est}A_{est}$ deviates from $\rho_{FM}\lambda_{FM}$ by only a small amount. Although Eq. 5 reproduces the correct value of λ_N for large d, a considerable discrepancy arises at small d, with λ_{eff} diverging from λ_N. The extent of the discrepancy is highly dependent on the assumed value of $R_{est}A_{est}$. In particular, the sensitivity to R_IA_I in these FM/NM devices means that even modest (approximately ± 10 %) errors in contact resistance can greatly alter the extracted value of τ_{eff} when fitting, particularly when spin sinking is appreciable. This in turn causes considerable under- or over-estimation of λ_N. In practice, the variations in R_I are probably the most significant factor influencing the dispersion in λ_{eff} among samples prepared in different growths.

The impact of such deviations in R_I must be taken in the context of the magnitude of spin sinking effects. Naturally, substantial R_I (*i.e.*, $R_I \gg R_N$) will greatly reduce many of the difficulties highlighted, and in this limit uncertainties in R_I will not impact the extracted λ_N appreciably. However, if R_I is small, such that spin sinking is still appreciable (as is still the case when $R_IA_I \sim 10\, \rho_{FM}\lambda_{FM}$ for all-metallic devices), deviations in this value can still cause considerable discrepancies in λ_N. As shown in Fig 5b for $R_IA_I = 10\, \rho_{FM}\lambda_{FM}$, the magnitude of this impact is surprisingly large, even in the case where $R_I > R_{FM}$. Only in the limit $R_IA_I \gg 10\, \rho_{FM}\lambda_{FM}$ do these variations become significantly smaller than the $R_I = 0$ scenario discussed. This is most readily seen in Fig 5c, where λ_{eff}/λ_N is shown as a function of R_IA_I for $d = \lambda_N$ and $\rho_{FM}\lambda_{FM} = 0.52$ fΩm^2. These data are obtained in an identical manner to that of Figs. 5a and b: an estimated interface resistance is used, in this case fixing $R_{est}A_{est} = R_{FM}A_I + 2\, R_IA_I$ (*i.e.*, miscalculating R_I by a factor of two). The data show substantial underestimation of λ_N when R_IA_I is comparable to $\rho_{FM}\lambda_{FM}$, as would naively be anticipated. What is perhaps surprising, however, is the extent to which underestimation occurs even at what may be considered much higher values of R_IA_I ($R_IA_I \sim 10\rho_{FM}\lambda_{FM}$).

Finally, we discuss the case of anisotropic spin sinking, as recently introduced in Ref. [6]. Anisotropic sinking accounts for the different spin currents drawn by the FM for spins in the N that are polarized longitudinally or transverse with respect to the FM magnetization. The two distinct mechanisms account for the uncorrelated spin-flip scattering events which relax the longitudinal accumulation, and the (typically shorter) precessional relaxation of the transverse spins. The degree of transverse sinking is parameterized by the transverse FM spin resistance, or, alternatively, the interfacial spin mixing conductance $G_{\uparrow\downarrow}$. As anticipated, complete agreement exists between such a treatment and Eq. 5 in the limit of isotropic spin sinking, *i.e.*, when longitudinal and transverse lifetimes are identical, so that $G_{\uparrow\downarrow} = 1/2\rho_{FM}\lambda_{FM}$. Although some degree of anisotropy in the spin sinking rate is anticipated,[34–39] our results can be fit successfully without the inclusion of an anisotropic term, and we therefore do not include the additional parameter in our 3-D simulations. We emphasize that although such anisotropic sinking effects are in principle more easily observed at smaller separations, the sensitivity to systematic errors in λ_N, *d*, R_{FM} and H_K, in addition to the limitations of 1-D modelling in the small *d* regime, make the existence of an anisotropic contribution difficult to establish for FM/N NLSVs. This is particularly true when one considers the fact that the measured $G_{\uparrow\downarrow}$ values are comparable to $1/A_{FM}R_{FM}$ for the FM/N combinations studied here.[6,40,41] In summary, although a separate transverse spin sinking term can be added, as suggested by the authors of Ref. [6], we find that there is no need to do so in the current case.

As one further point of consideration, we note that the difficulties with fitting discussed here are further compounded by the finite FM contact anisotropy H_K. As $d \rightarrow 0$, the Hanle curve widens to the point that it extends beyond H_K. At these magnetic fields the Hanle curve shape becomes extremely sensitive to the rotation of the FMs OOP. Without measuring *both* R_P and R_{AP}, while *also* knowing the precise field dependence of the magnetization rotation, the resulting systematic error in fitting experimental Hanle curves for $d \ll \lambda_N$ precludes the determination of λ_N with reasonable precision. For the FM/N combinations studied here, the Hanle curve width becomes an appreciable fraction of H_K for $d <$ 500 nm, setting the lower limit of d for an acceptable measurement of τ_s. We therefore do not consider curves generated at smaller separations and believe a similar limitation applies to other studies of metallic lateral spin valves.

In conclusion, we have demonstrated, by exploring the dependence of non-local measurements on contact separation, the effect of contact-induced spin sinking in lateral spin valves. The spin sinking effect leads to an underestimation of λ_N as determined from Hanle measurements in all-metallic devices. Although sinking is present at all separations, the underestimation is most pronounced when $d < \lambda_N$, resulting in a monotonic decrease (with decreasing d) of the effective diffusion length extracted from Hanle measurements. The observed trends are reproduced over the separations probed using models that consider isotropic spin sinking. Our 3-D simulations show that the effective diffusion length does not tend to $\lambda_N R_{FM}/R_N$ as the $d \rightarrow 0$ limit is reached, as anticipated from 1-D modelling, but instead saturates at a considerably larger value. More generally we find that the sensitivity of spin sinking models to interface resistance, FM contact magnetization rotation, and other device parameters, produces significant systematic errors when fitting Hanle curves, particularly when $d < \lambda_N$. This highlights the difficulties of using such a method to determine λ_N in all-metallic devices. The most reliable values of λ_N are obtained from measurements of the *magnitude* of $\Delta R_{NL}(d)$, extending out to separations of several diffusion lengths. Conversely, using Hanle or NLSV measurements to probe R_{FM} reliably will require experiments in the limit $d \ll \lambda_N$ in order to be sensitive to spin sinking effects.

Acknowledgments: This work was funded by Seagate Technology Inc. and the University of Minnesota (UMN) NSF MRSEC under DMR-1420013, as well as NSF DMR-1104951 and NSF DMR-1507048. L.O'B. acknowledges a Marie Curie International Outgoing Fellowship within the 7th European Community Framework Programme (project no. 299376). Parts of this work were carried out in the UMN Characterization Facility and Minnesota Nano Center, which receive partial support from the NSF MRSEC and NSF NNIN programs, respectively.

References

[1] M. Johnson and R.H. Silsbee, Phys. Rev. Lett. **55**, 1790 (1985).

[2] F.J. Jedema, A.T. Filip, and B.J. van Wees, Nature **410**, 345 (2001).

[3] Y. Fukuma, L. Wang, H. Idzuchi, S. Takahashi, S. Maekawa, and Y. Otani, Nat. Mater. **10**, 527 (2011).

[4] F.J. Jedema, H.B. Heersche, A.T. Filip, J.J.A. Baselmans, and B.J. van Wees, Nature **416**, 713 (2002).

[5] W. Han, K. Pi, K.M. McCreary, Y. Li, J.J.I. Wong, A.G. Swartz, and R.K. Kawakami, Phys. Rev. Lett. **105**, 167202 (2010).

[6] H. Idzuchi, Y. Fukuma, S. Takahashi, S. Maekawa, and Y. Otani, Phys. Rev. B **89**, 081308 (2014).

[7] F. Volmer, M. Drögeler, E. Maynicke, N. von den Driesch, M.L. Boschen, G. Güntherodt, C. Stampfer, and B. Beschoten, Phys. Rev. B **90**, 165403 (2014).

[8] H. Idzuchi, A. Fert, and Y. Otani, Phys. Rev. B **91**, 241407 (2015).

[9] T. Maassen, I.J. Vera-Marun, M.H.D. Guimarães, and B.J. van Wees, Phys. Rev. B **86**, 235408 (2012).

[10] E. Sosenko, H. Wei, and V. Aji, Phys. Rev. B **89**, 245436 (2014).

[11] M. Drögeler, C. Franzen, F. Volmer, T. Pohlmann, L. Banszerus, M. Wolter, K. Watanabe, T. Taniguchi, C. Stampfer, and B. Beschoten, Nano Lett. **16**, 3533 (2016).

[12] W. Amamou, Z. Lin, J. van Baren, S. Turkyilmaz, J. Shi, and R.K. Kawakami, APL Mater. **4**, 032503 (2016).

[13] M. Popinciuc, C. Józsa, P.J. Zomer, N. Tombros, A. Veligura, H.T. Jonkman, and B.J. van Wees, Phys. Rev. B **80**, 214427 (2009).

[14] T. Valet and A. Fert, Phys. Rev. B **48**, 7099 (1993).

[15] T. Kimura, T. Sato, and Y. Otani, Phys. Rev. Lett. **100**, 066602 (2008).

[16] H. Zou and Y. Ji, Appl. Phys. Lett. **101**, 082401 (2012).

[17] G. Mihajlović, J.E. Pearson, S.D. Bader, and A. Hoffmann, Phys. Rev. Lett. **104**, 237202 (2010).

[18] N. Poli, M. Urech, V. Korenivski, and D.B. Haviland, J. Appl. Phys. **99**, 08H701 (2006).

[19] L. O'Brien, M.J. Erickson, D. Spivak, H. Ambaye, R.J. Goyette, V. Lauter, P.A. Crowell, and C. Leighton, Nat. Commun. **5**, 3927 (2014).

[20] T. Wakamura, N. Hasegawa, K. Ohnishi, Y. Niimi, and Y. Otani, Phys. Rev. Lett. **112**, 036602 (2014).

[21] S. Garzon, I. Žutić, and R. Webb, Phys. Rev. Lett. **94**, 176601 (2005).

[22] F. Bakker, A. Slachter, J.-P. Adam, and B. van Wees, Phys. Rev. Lett. **105**, 136601 (2010).

[23] S. Takahashi and S. Maekawa, Phys. Rev. B **67**, 052409 (2003).

[24] J. Bass and W.P. Pratt, J. Phys. Condens. Matter **19**, 183201 (2007).

[25] L. O'Brien, D. Spivak, J.S. Jeong, K.A. Mkhoyan, P.A. Crowell, and C. Leighton, Phys. Rev. B **93**, 014413 (2016).

[26] F.J. Jedema, M. V. Costache, H.B. Heersche, J.J.A. Baselmans, and B.J. van Wees, Appl. Phys. Lett. **81**, 5162 (2002).

[27] A. Aharoni, J. Appl. Phys. **83**, 3432 (1998).

[28] The relationship between the spin and charge diffusion constants is a more open question in two-

dimensions, but experimental tests (based on Hanle measurements) indicate that they are approximately the same in graphene. See T. Maassen, F. K. Dejene, M. H. D. Guimarães, C. Józsa, and B. J. van Wees, Phys. Rev. B 83, 115410 (2011).

[29] E. Villamor, L.E. Hueso, and F. Casanova, J. Appl. Phys. **117**, 223911 (2015).

[30] M. Furis, D.L. Smith, S. Kos, E.S. Garlid, K.S.M. Reddy, C.J. Palmstrøm, P.A. Crowell, and S.A. Crooker, New J. Phys. **9**, 347 (2007).

[31] F. Jedema, M. Nijboer, A. Filip, and B. van Wees, Phys. Rev. B **67**, 085319 (2003).

[32] T. Kimura, J. Hamrle, and Y. Otani, Phys. Rev. B **72**, 014461 (2005).

[33] N. Theodoropoulou, A. Sharma, T. Haillard, R. Loloee, W.P. Pratt Jr., J. Bass, J. Zhang, and M.A. Crimp, IEEE Trans. Magn. **43**, 2860 (2007).

[34] A. Ghosh, S. Auffret, U. Ebels, and W.E. Bailey, Phys. Rev. Lett. **109**, 127202 (2012).

[35] T. Taniguchi, S. Yakata, H. Imamura, and Y. Ando, IEEE Trans. Magn. **44**, 2636 (2008).

[36] T. Taniguchi, S. Yakata, H. Imamura, and Y. Ando, Appl. Phys. Express **1**, 031302 (2008).

[37] S. Nonoguchi, T. Nomura, and T. Kimura, Phys. Rev. B **86**, 104417 (2012).

[38] S. Zhang, P.M. Levy, and A. Fert, Phys. Rev. Lett. **88**, 236601 (2002).

[39] M.D. Stiles and A. Zangwill, Phys. Rev. B **66**, 14407 (2002).

[40] Y. Tserkovnyak, A. Brataas, G. Bauer, and B. Halperin, Rev. Mod. Phys. **77**, 1375 (2005).

[41] F.D. Czeschka, L. Dreher, M.S. Brandt, M. Weiler, M. Althammer, I.-M. Imort, G. Reiss, A. Thomas, W. Schoch, W. Limmer, H. Huebl, R. Gross, and S.T.B. Goennenwein, Phys. Rev. Lett. **107**, 046601 (2011).

Figures

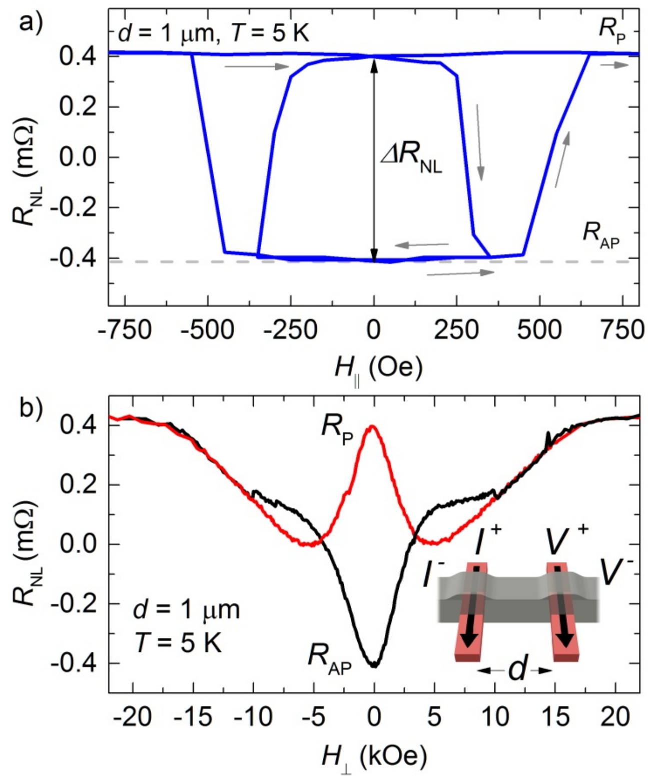

Figure 1. (color online) a) In-plane magnetic field, $H_{||}$, dependence of the non-local resistance, R_{NL}, for a d = 1 μm Fe/Al NLSV at T = 5 K. Indicated are the parallel (R_P) and antiparallel (R_{AP}) non-local resistances and the spin accumulation signal, $\Delta R_{NL} = R_P - R_{AP}$. Gray arrows show the evolution of $H_{||}$ from negative to positive saturation. b) Out-of-plane magnetic field, $H_\perp$, dependence of R_{NL} for the same d = 1 μm, Fe/Al NLSV at T = 5 K. Inset: Schematic of NLSV geometry. A field-independent background of -0.632 mΩ has been subtracted from a) and b).

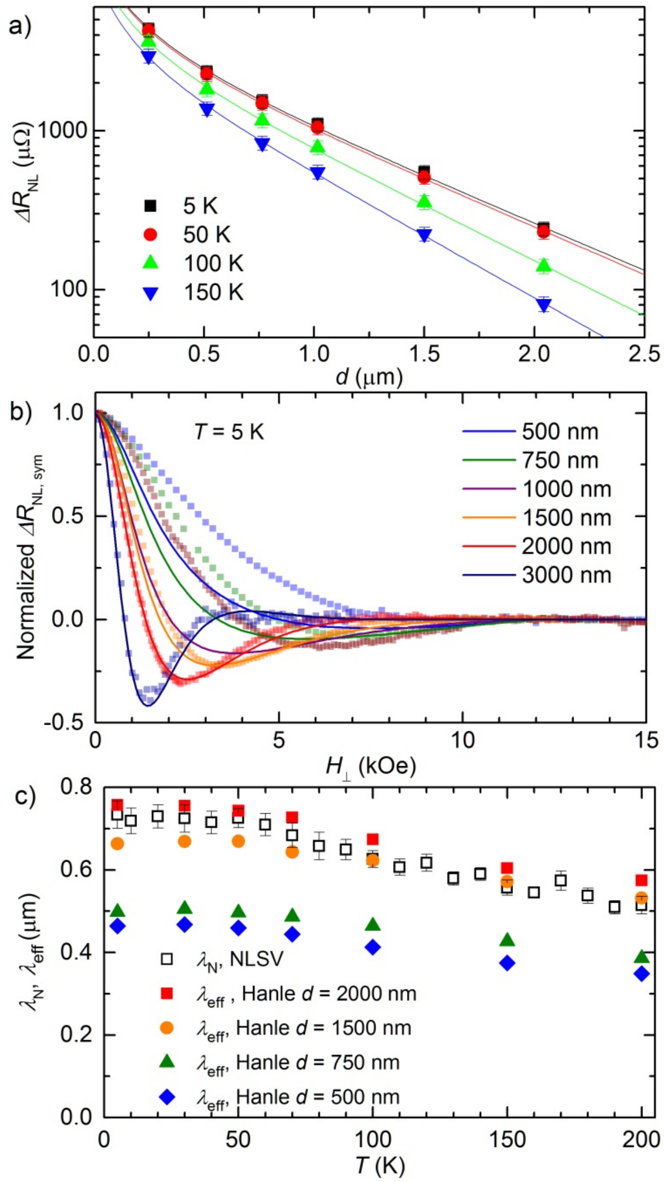

Figure 2. (color online) a) Dependence of ΔR_{NL} on separation d for various T in Fe/Al NLSVs. Solid lines are fits to the 1-D spin diffusion model discussed in the text. b) $\Delta R_{NL}(H_\perp)$ for various d at T = 5 K, normalized to $\Delta R_{NL}(H_\perp = 0\ \mathrm{Oe})$. Data are taken for both positive and negative $H_\perp$. The symmetric component, $\Delta R_{NL,sym} = [\Delta R_{NL}(H_\perp) + \Delta R_{NL}(-H_\perp)]/2$, is shown. Solid lines show the *predicted* $\Delta R_{NL}(H_\perp)$ based on a 1-D analytical Hanle model, *not* accounting for back-diffusion of spins into the FMs. c) $\lambda_N(T)$ from NLSV $\Delta R_{NL}(d)$ measurements (open black squares), compared to effective values ($\lambda_{eff}(T)$) extracted from Hanle curves obtained on the same devices [the same batch as used for (a)]

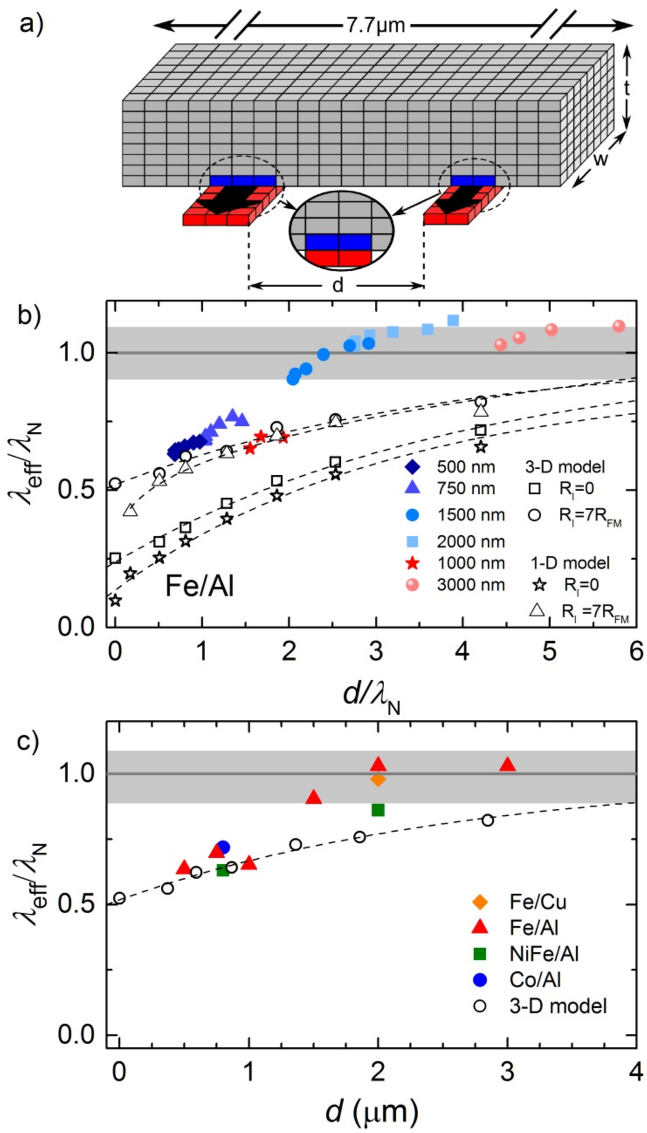

Figure 3. (color online) a) Schematic illustrating the approach to 3D modelling, with the 3D grid showing the discretization of the sample. Only the volume in the vicinity of the FM contacts is shown. The red cells are the FM. The blue cells are those in which the spin relaxation rate in N is modified, as described in the text. b) λ_{eff}/λ_N *vs*. reduced separation d/λ_N in Fe/Al NLSVs. Data are shown for six *d* values at various *T*, the closed blue and red symbols denoting the two batches of devices tested. Black open squares and open circles indicate results from our 3D modelling including spin sinking in the FMs, with $R_I = R_{FM}$ and $R_I = 7\,R_{FM}$, respectively. Black stars show the 1-D modelling of Maassen *et al.*[9], with open triangles showing the case of $R_I = 7R_{FM}$. Dashed lines are guides to the eye. c) λ_{eff}/λ_N *vs*. *d* for various FM/N combinations at *T* = 5 K. Black open circles again indicate results from our modelling including spin sinking. In b) and c) the gray band marks the tunnel barrier limit, the width indicating the systematic error in λ_N from spin-valve measurements of $\Delta R_{NL}(d)$.

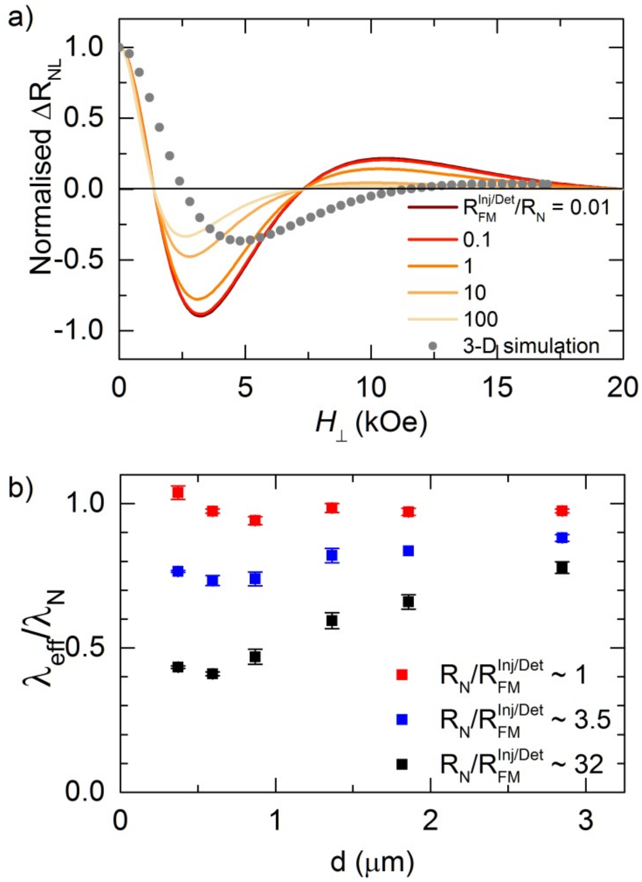

Figure 4 (color online) a) Normalized ΔR_{NL} vs $H_{\perp}$ from a 1-D model assuming only longitudinal spin sinking for a $d = 2$ μm Fe/Al NLSV. Curves are shown for R_I/R_N varying from 0.01 to 100. Shown for comparison are data from a 3-D simulation assuming isotropic sinking (gray circles). b) λ_{eff}/λ_N extracted from fitting 3-D simulations using a 1-D longitudinal sinking model for various R_I/R_N, using identical material parameters and $\lambda_N = 733$ nm.

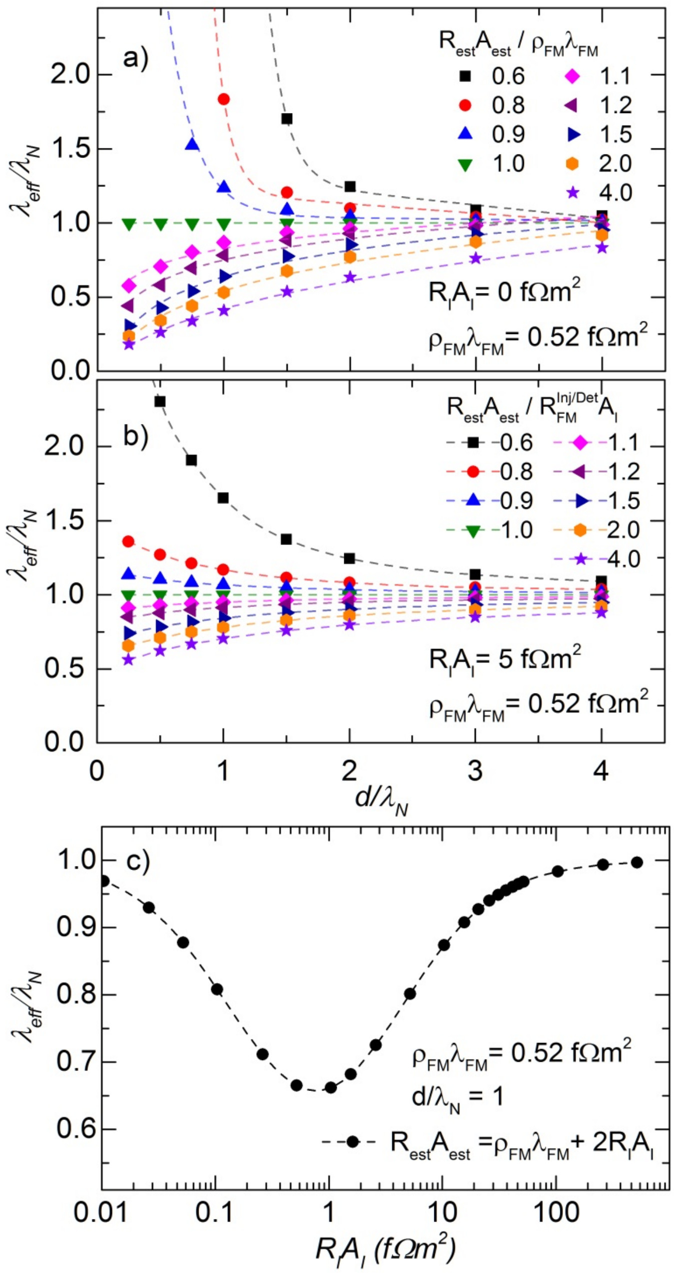

Figure 5 (color online) a) and b) λ_{eff}/λ_N extracted from fitting a single set of model data generated using the 1-D isotropic sinking model (with λ_N = 733 nm, $\rho_{FM}\lambda_{FM}$ = 0.52 fΩm^2). Shown are the cases for a) $R_I = 0$ and b) $R_I = 5$ fΩm^2. Each fit is performed using the *same* model, but while constraining the total FM contact spin resistance to various estimated values, $R_{est}A_{est}$ Estimated values are normalized to the true FM spin resistance, $R_{FM}^{Inj/Det}$. c) λ_{eff}/λ_N vs R_IA_I extracted using a similar method to a) and b) for the case where $d = \lambda$, $\rho_{FM}\lambda_{FM}$ = 0.52 fΩm^2, where a constant overestimation of R_I is made during fitting ($R_{est}A_{est} = \rho_{FM}\lambda_{FM} + 2R_IA_I$. Dashed lines provide a guide to the eye.

Appendix A

As discussed in the main text, λ_{eff} can be determined by fitting the symmetrized Hanle signal $\Delta R_{NL}(H_{\perp})$ to Eq. 2, which ignores the back-diffusion of spins into the FM. These fits are shown separately here to distinguish them clearly from the solid curves in Fig. 2b, which are the Hanle curves that would be expected based on the actual spin diffusion length λ_N, as determined from fitting the separation dependence of the non-local spin valve signal.

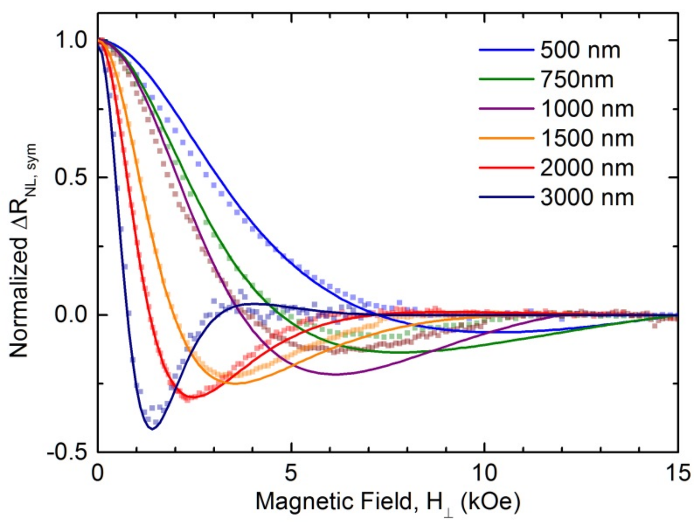

Figure A1 $\Delta R_{NL}(H_{\perp})$ for various d at T = 5 K, normalized to $\Delta R_{NL}(H_{\perp} = 0\ \mathrm{Oe})$. Data are taken for both positive and negative $H_{\perp}$; only the symmetric component, $\Delta R_{NL,sym} = [\Delta R_{NL}(H_{\perp}) + \Delta R_{NL}(-H_{\perp})]/2$, is shown. Solid lines show the *fitted curves* based on a 1-D analytical Hanle model, not accounting for back-diffusion of spins into the FMs. Extracted values of λ_{eff} are shown in Fig. 2c of the main text.

Appendix B

Here we derive Eq. 4 in the main text, which accounts for the spin current flowing into the ferromagnet by introducing an enhanced spin relaxation rate f_s^* in the simulation cells adjacent to the interface. The FM is assumed to occupy the half-space $z < 0$. We assume a spin-dependent electrochemical splitting

$$\Delta\mu = \mu_{\uparrow} - \mu_{\downarrow} \tag{B1}$$

at the interface between N and FM. This can be related to the spin current q_0 (which has dimensions of number per unit area per unit time) flowing into the ferromagnet by

$$q_0 = -\frac{\Delta\mu}{e^2 R_{FM}}, \tag{B2}$$

where e is the electron charge and $R_{FM} = \rho_{FM}\lambda_{FM}$ is the spin resistance of the ferromagnet. Assume a cell at the interface has a cross-sectional area A and height Δz. The spin flowing out of this cell into the ferromagnet is simply $q_0 A$. The rate of change of the spin accumulation per unit volume in the cell is

$$\frac{\partial(n_\uparrow - n_\downarrow)}{\partial t} = \frac{q_0}{\Delta z} - \frac{n_\uparrow - n_\downarrow}{\tau_s}, \tag{B3}$$

where the first term on the right-hand side is the contribution from the spin current flowing across the interface and the second term is the ordinary spin relaxation within the cell, with τ_s the spin relaxation time in the N. The left-hand side of Eq. B3 can be converted to an electrochemical potential splitting using

$$\Delta\mu = \mu_\uparrow - \mu_\downarrow = \left(\frac{\partial\mu}{\partial n}\right)(n_\uparrow - n_\downarrow), \tag{B4}$$

so that Eq. B3 can be rewritten as

$$\frac{\partial\Delta\mu}{\partial t} = \left(\frac{\partial\mu}{\partial n}\right)\frac{q_0}{\Delta z} - \frac{\Delta\mu}{\tau_s} = -\rho_N D_N \frac{\Delta\mu}{\Delta z R_{FM}} - \frac{\Delta\mu}{\tau_s}, \tag{B5}$$

where we have used Eq. B2 and the Einstein relation $\partial\mu/\partial n = \rho e^2 D$. Using the definition $\lambda_N = \sqrt{D_N\tau_S}$,

$$\frac{\partial\Delta\mu}{\partial t} = -\left(\frac{\rho_N\lambda_N^2}{\tau_s}\frac{1}{\Delta z R_{FM}} + \frac{1}{\tau_s}\right)\Delta\mu = -\left[1 + \left(\frac{\rho_N\lambda_N}{\rho_{FM}\lambda_{FM}}\right)\left(\frac{\lambda_N}{\Delta z}\right)\right]\frac{\Delta\mu}{\tau_s}. \tag{B6}$$

Equation B6 has the form

$$\frac{\partial\Delta\mu}{\partial t} = -f_s^*\Delta\mu, \tag{B7}$$

where f_s^* is the effective spin relaxation rate given in Eq. 4 of the main text. Note that in the tunnel barrier case, the spin resistance in the denominator of the second term in brackets is effectively infinite, and we would then recover the expected result $f_S^* = \tau_s^{-1}$.